Testing the Three Step Excited State Proton Transfer Model by the Effect of an Excess Proton

Rinat Gepshtein, Pavel Leiderman, Liat Genosar, and Dan Huppert*

Raymond and Beverly Sackler Faculty of Exact Sciences, School of Chemistry, Tel Aviv University, Tel Aviv 69978, Israel

Received: June 27, 2005; In Final Form: August 31, 2005

In a previous work, we proposed an extended model for intermolecular excited-state proton transfer to the solvent. The model invoked an intermediate species, the contact ion-pair $RO^-\cdots H_3O^+$, where a proton is strongly hydrogen bonded to the conjugated photabase RO^-*. In this study we tested the extended model by measuring the transient absorption and emission of 8-hydroxypyrene-1,3,6-trisulfonate (HPTS) in an aqueous solution in the presence of a large concentration of mineral acids. In a neutral pH solution, the pump−probe signal consists of three time components, <1, 4, and 100 ps. The 4 ps time component, with a relative amplitude of about 0.3, was attributed to the formation of the contact ion-pair and the long 100 ps component to the dissociation of the ion-pair to a free proton and RO^-*. In the presence of acid, the recombination of an excess proton competes with the geminate recombination. At a high acid concentration, the recombination process alters the time-dependent concentrations of the reactant, product and intermediate contact ion-pair. We observed that when the acid concentration increases, the amplitude of both the long and intermediate time components decreases. At about 3 M of acid, both components almost disappear. Model calculations of the acid effect on the transient HPTS signal indeed showed that the amplitude of the intermediate time component decreases as the excess proton concentration increases.

Introduction

Proton-transfer reactions are ubiquitous in chemical and biological processes.[1−4] Over the last two decades, intermolecular proton transfer in the excited state (ESPT) has been studied extensively both theoretically and experimentally and provided valuable information about the mechanism and nature of acid−base reactions.[5−11]

To initiate these reactions, protic solvent solutions of suitable organic molecules are irradiated by short (femtosecond−picosecond) laser pulses.[12−14] Consequently, the excited-state molecules dissociate very rapidly by transferring a proton to a nearby solvent molecule.

8-Hydroxypyrene-1,3,6-trisulfonate, (HPTS or pyranine) is a photoacid commonly used in the study of the ESPT process. The RO^- form is quadruply negatively charged. Thus, the reversible geminate recombination process is strongly enhanced relative to a singly charged photoacid like 2-naphthol. We have studied HPTS ESPT for many years.[15−17] The proton-transfer rate could be determined either by the initial decay time of the time-resolved fluorescence of the protonated form (ROH) measured at 440 nm or by the slow rise-time of the emission of the deprotonated species (RO^-).

Over the past decade, we used a model for an intermolecular ESPT process that accounts for the geminate recombination of the transferred proton. In this model, the overall dissociation process can be subdivided into the two consecutive steps of reaction and diffusion. In the reactive stage, a rapid short-range charge separation occurs and a solvent-stabilized ion pair is formed. This is followed by a diffusive stage, when the two ions withdraw from each other due to their thermal random motion. The reverse process is geminate recombination (neutralization) of the two separated ions either by the direct collapse of the ion pair, or following a geminate reencounter of the solvated "free" ions.

SCHEME 1

$$ROH^* \underset{k_r}{\overset{k_{PT}}{\rightleftharpoons}} [RO^-\cdots H^+]_{(r=a)} \overset{DSE}{\rightleftharpoons} RO^- + H^+$$

In a previous study, we measured using time-resolved emission and absorption spectroscopies the ESPT process from HPTS to water. We used the time correlated single proton counting TCSPC and femtosecond pump−probe techniques. On the basis of the experimental data and the experimental data presented in the recent papers of Prayer et al.[10] and Tran-Thi et al.[11] and model calculations made by Ando et al.,[18] we adopted the framework of the model that was originally proposed by both Eigen[4] and Weller[3] for the intermolecular ESPT processes. The model extends our previous diffusion-assisted excited-state proton-transfer model to include an additional reactive step (see Schemes 1 and 2).

The excited protonated acid ROH* dissociates first to a contact ion-pair, consisting of an anion and a hydrogen-bonded hydrated proton complex which we designate H_3O^+. The contact ion-pair $RO^-\cdots H_3O^+$ exhibits about the same UV−vis spectroscopic signature as the RO^- emission band of the separated ion-pair and the free RO^-. Our model accounts for the following experimental observations:

1. The time-dependent concentration of both ROH* and RO^-* is biphasic with time constants of ∼4 and 100 ps and relative amplitudes of about 0.3 and 0.7, respectively. The ROH concentration decays while the RO^- concentration increases.

2. A two reactive step mechanism, followed by a diffusion step, fits the experimental data well. The acid first dissociates

* Corresponding author. E-mail: huppert@tulip.tau.ac.il. Fax/telephone: 972-3-6407012.

10.1021/jp053479w CCC: $30.25
Published on Web 09/30/2005

SCHEME 2

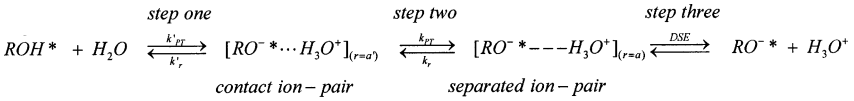

to form a contact ion pair $RO^{-}*\cdots H_3O^{+}$ with a time constant of about 15 ps. The equilibrium constant of the first step is about 0.5. Thus, the concentration of the protonated form, ROH*, decays at a short time of about 4 ps to an equilibrium value of about 0.7.

3. The 4 ps component observed in the ultrafast experiments is somewhat misleading for deducing the actual rate of dissociation. The 4 ps component arises from the faster recombination rate constant. The overall observed fast rate constant is given as a sum of the forward and backward rate constants.

4. In the second reactive step, the contact ion-pair separates by further solvation of both the RO^{-} and the proton. The rate of this step is slow, $\tau_{PT} = 28$ ps.

5. The third step involves the diffusion-assisted reversible geminate recombination of the proton with the excited conjugated base.

Recently, Mohammed et al.[19] studied, using femtosecond midinfrared spectroscopy, the vibrational-mode characteristics of the electronic state involved in the excited-state dynamics of HPTS that ultimately led to efficient proton transfer in H_2O. They concluded that, for HPTS photoacid, the first excited singlet state appears to have charge-transfer properties in water within a time resolution of 150 fs whereas, in aprotic DMSO, the photoacid appears to be in a nonpolar electronic excited state. They argued that previously observed short time-components in UV/vis pump−probe studies should be related to solvation dynamics rather than to intermediates in the proton-transfer process. Thus, their conclusion contradicts our model and similar models,[10,11] which indicate that proton transfer occurs in HPTS during the early stages.

In this study, we further explore the validity of the extended proton dissociation model by monitoring the "acid" effect by introducing a large concentration of strong mineral acid to the solution. The excess protons compete with the geminate proton to recombine reversibly with $RO^{-}*$ and re-form the excited photoacid, ROH*.

$$RO^{-}* + H^{+}_{(excess)} \rightarrow ROH^{*},\ RO^{-}* + H^{+}_{(geminate)} \rightarrow ROH^{*} \quad (1)$$

At large acid concentrations, the recombination process alters the time-dependent concentrations, of the reactant, product, and intermediate contact ion-pair.

Experimental Section

Time-resolved fluorescence was acquired using the time-correlated single-photon counting (TCSPC) technique, the method of choice when sensitivity, large dynamic range, and low intensity illumination are important criteria in fluorescence decay measurements.

For excitation, we used a cavity dumped Ti:sapphire femtosecond laser, Mira, Coherent, which provides short, 80 fs, pulses of variable repetition rate, operating at the SHG frequency, over the spectral range of 380−400 nm with the relatively low repetition rate of 500 kHz. The TCSPC detection system is based on a Hamamatsu 3809U, photomultiplier and Edinburgh Instruments TCC 900 computer module for TCSPC. The overall instrumental response was about 35 ps (fwhm). Measurements were taken at 10 nm spectral width. The excitation pulse energy was reduced by neutral density filters to about 10 pJ. We checked the sample's absorption prior to and after time-resolved measurements. We could not find noticeable changes in the absorption spectra due to sample irradiation.

For the pump−probe experiments reported, we used an amplified femtosecond Ti:sapphire laser system. In brief, laser pulses (50 fs duration, centered near 800 nm with pulse energy of ~600 μJ) at a 1 kHz repetition rate were generated by a Ti:sapphire-based oscillator (Coherent Mira seed) and amplified by a multipass Ti:sapphire amplifier (Odin Quantronix). Samples were excited by the second harmonic of the amplified laser (~400 nm). To obtain probe pulses, we generated a super continuum by focusing 1 μJ of either the 800 or 400 nm (the second harmonic of 800 nm) pulse onto a 2 mm thick sapphire window. The continuum generated with the 400 nm beam provided a probe pulse in the region of 410−500 nm. The probe beam signal was measured by a combination of a chopper/lockin amplifier and computer averaging. Interference filters of 8 nm fwhm bandwidth at the proper wavelength were used in front of the probe beam detector, a silicon photodiode. Samples were placed in a rotating optical cell to avoid degradation. The HPTS concentration in the rotating cell was 3×10^{-4} M.

Steady-state fluorescence spectra were taken using a Fluoro-Max (Jobin Yvon) spectrofluorimeter. HPTS, laser grade, was purchased from Kodak. Perchloric acid, 70% reagent grade, was purchased from Aldrich. For steady-state fluorescence measurements we used solutions of $\sim 2 \times 10^{-5}$ M of HPTS.

The Old Reversible Diffusion-Influenced Two Step Model of Pines, Huppert, and Agmon. Scheme 1 shows the "old" model schematically.[20−26]

The first step is described by back-reaction boundary conditions k_{PT} and k_r. This is followed by a diffusional second step, in which the hydrated proton is removed from the parent molecule solvation shell. In the continuous diffusion approach, one describes this dissociation reaction second step by a spherically symmetric three-dimensional diffusion equation, the Debye−Smoluchowski equation (DSE).[27,28] k_{PT} and k_r are the "intrinsic" dissociation and recombination rate constants at the contact sphere radius, a. k_{PT} determines the initial slope of the decay curves: the larger k_{PT}, the faster the initial exponential decay. The intrinsic recombination rate constant, k_r, does not affect the behavior at $t \rightarrow 0$, but determines the magnitude of the long-time tail. Quantitative agreement was obtained between theory and experiment. A detailed description of the model, as well as the fitting procedure, is given in refs 17, 21, and 29.

The New Model for ESPT. In our previous paper,[30] we extended our previous diffusion-assisted excited-state proton-transfer model to include an additional reactive step (see Scheme 1). A simple and straightforward description of the modified ESPT model is given by Scheme 2, where R is an organic radical and $[RO^{-}*\cdots H_3O^{+}]$ is the contact ion pair formed between the molecular anion RO^{-} and the proton H^{+}, separated by a short distance a'. k'_{PT} and k'_r are the forward and reverse rate constants of the first step, respectively. Our old model covers the second and third steps. Details of our old model including the second reactive step and the diffusive part were given in the previous section.

The excited protonated acid ROH* dissociates first to a contact ion-pair, consisting of an anion and a hydrogen bonded

hydrated proton complex which we designate H_3O^+. The contact ion-pair $RO^-{}^*\cdots H_3O^+$ exhibits about the same spectroscopic signature as the RO^- emission band of the separated and solvated ion-pair. The fluorescence band is broad, is asymmetric, and has a peak at about 512 nm. An important finding of the model fitting to the experimental data imposes that the equilibrium constant of the first step in the dissociation process is about 0.5. Thus, the time-dependent concentration of the contact ion pair is small at all times. The decrease of the ROH concentration in the first few picoseconds is rather small, only 30%. This decrease in excited ROH concentration is easily measured by femtosecond techniques such as fluorescence upconversion or pump−probe. In the TCSPC signal of the ROH fluorescence, measured at 435 nm, the first dissociation step should decrease the ROH signal. However, due to limited time resolution, this decrease cannot be detected. In the rise-time of the RO^- TCSPC signal measured at $\lambda > 520$ nm, a short rise-time component of about 22% is followed by a long 100 ps rise-time. It appears as an immediate rise-time within the instrument response function of the TCSPC system. We used a simple kinetic model[31] to display the main features of the ESPT process:

$$A \underset{k'_r}{\overset{k'_{PT}}{\rightleftharpoons}} B \underset{k_r}{\overset{k_{PT}}{\rightleftharpoons}} C$$

where A denotes the photoacid, B the ion pair, and C the separated ion pair and the diffusive free $RO^-{}^*$. In our case, the fluorescence band shape and position of the intermediate product B ($RO^-{}^*\cdots H_3O^+$) and the C species ($RO^-{}^*\text{- - -}H_3O^+$) are about the same, and thus, the measured fluorescence is from either the excited photoacid ROH* with a peak at 440 nm or the combined B + C fluorescence at 512 nm arising from RO^-. The ABC model does not include the last step, the diffusion assisted geminate-recombination of the proton with the conjugated base. The time-dependent concentrations of A (ROH), B ($RO^-\cdots H^+$), and C ($RO^-\text{- - -}H^+$) are given in Appendix A.

Since the first step rate constants are larger than the second step rate constants, k'_{PT}, $k'_r \gg k_{PT}$, k_r, the decrease of the population of ROH* is biphasic, the first step involves the reduction of the ROH* population by ~30% to form a contact ion-pair. The contact ion-pair concentration is limited since the equilibrium constant, K'_{eq}, is about 0.5 and the second step involves much slower processes. The recombination rate constants k_r and k'_r are modified by the acid concentration. In general, they can be considered as pseudo-first-order rate constants with respect to the acid concentration. Appendix B deals with the dependence of the recombination rate constants on the acid concentration.

Results

Steady-State Emission. Figure 1a shows the steady-state emission spectra of HPTS in the presence of low concentrations of $HClO_4$ in the concentration range 10^{-6} M $< c <$ 0.6 M. The emission spectra consist of two broad structurless bands positioned at about 435 nm and 510 nm. The photoacid form ROH emits at 435 nm and RO^- at 510 nm. The emission spectra in the figure are normalized to the deprotonated form RO^-. As the acid concentration increases the intensity of the ROH emission band positioned at about 435 nm increases. At 0.8 M of $HClO_4$, the intensity of the ROH and RO^- fluorescence bands is almost equal.

Figure 1b shows the emission spectra of HPTS at high acid concentrations, 1 M $< c <$ 6 M. In this concentration range the spectra are normalized to the ROH band. The RO^- band

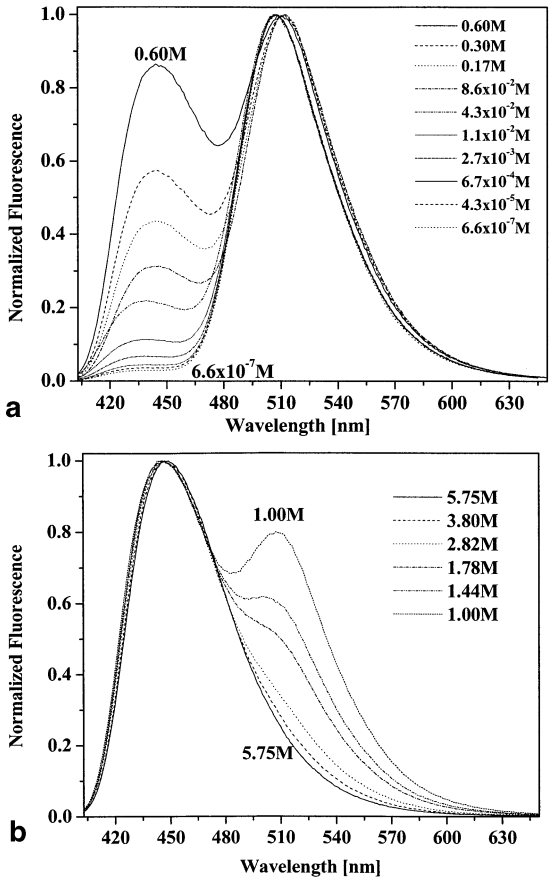

Figure 1. Steady-state emission spectra of HPTS in the presence of $HClO_4$: (a) $HClO_4$ concentration 10^{-6} M $< c \leq$ 0.6 M; (b) large acid concentration, 1 M $\leq c \leq$ 6 M.

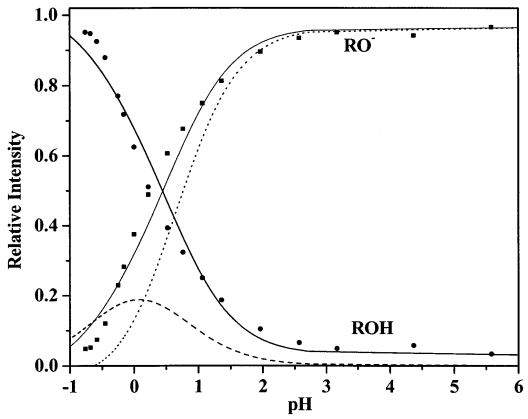

Figure 2. Relative fluorescence intensities of the RO^- (■) and ROH (●) forms of HPTS, as a function of acid concentration along with the calculation using the ABC model. Key: contact ion-pair (- - -), free RO^- (····), ROH (—), and combined RO^- and ion-pair probabilities (—).

intensity decreases as the acid concentration increases. At 6 M $HClO_4$, the RO^- emission band intensity is close to zero.

Figure 2 shows the plots of the relative fluorescence intensities of the RO^- and ROH forms of HPTS, as a function of $HClO_4$ concentration (symbols). The protonated and deprotonated fluorescence intensities were taken as the peak intensities at 440 and 510 nm respectively. At 0.8 M $HClO_4$, the fluorescence intensities of the RO^- and ROH are about equal. As will be shown in the Discussion, we are able to fit this fluorescence titration plot with our extended model while the single reactive step ESPT model fails to do so.

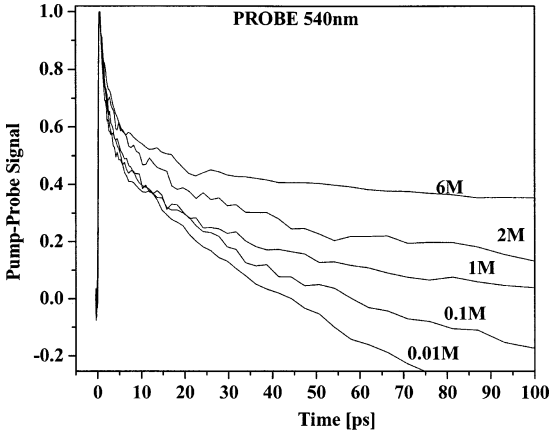

Figure 3. Pump−probe signal of HPTS probed at 540 nm in aqueous solutions of various concentrations of $HClO_4$.

TABLE 1: ABC Model Fitting Parameters for HPTS Pump−Probe Signal Probed at 540

$c(HClO_4)$ [M]	$k'_{PT} \times 10^9$ $[s^{-1}]^a$	$k'_r \times 10^9$ $[s^{-1}]^a$	$k_{PT} \times 10^9$ $[s^{-1}]^a$	$k_r \times 10^9$ $[s^{-1}]^a$	$\gamma_1 \times 10^{10}$ $[s^{-1}]^b$	$\gamma_2 \times 10^{11}$ $[s^{-1}]^b$
0.01	35	80	35	5	1.26	1.42
0.10	35	85	35	10	1.63	1.49
0.25	35	90	35	15.5	2.00	1.55
0.50	35	100	35	25	2.75	1.68
1.00	35	110	35	35	3.5	1.80
1.50	35	125	35	45	4.30	1.99
2.00	35	140	35	70	6.17	2.18
3.00	35	180	35	100	8.6	2.64
6.00	25[c]	210	35	120[c]	15	3.5

[a] Fitting parameter. [b] Calculated by eq a2α (Appendix A). [c] At 6 M $HClO_4$ the proton transfer and recombination rate constants decrease.

Pump—Probe Measurements. Figure 3 shows the pump−probe signal of HPTS in aqueous solutions of various concentrations of $HClO_4$. The sample was excited by the SHG of a mode-locked Ti:sapphire laser with ∼2 μJ 395 nm, 1 kHz pulses. The sample was probed at 540 nm where the stimulated emission of the RO^- band contributes to the signal. In aqueous solutions, the signal is positive at short times and negative at times longer than 50 ps. The time window in this experiment is quite narrow, providing us only 100 ps to examine the dynamics of the ESPT process. The signal consists of three major time components of <1, 4, and ∼100 ps (see Table 1). As the acid concentration increases, the long component's relative amplitude decreases. The intermediate component amplitude of 4 ps also decreases in solutions of acid with concentrations larger than 0.5 M. The amplitude of the fast, <1 ps, component is unaffected by the acid concentration.

Figure 4 shows the pump−probe signal probed at 430 nm of HPTS in aqueous solutions containing large concentrations of acids. At 430 nm, the protonated form, ROH, emission band is strong and hence the stimulated emission of the ROH contributes a major portion to the pump−probe signal. The signal at 430 nm is inverted in its sign to the signal measured at 540 nm. Both 430 and 530 nm pump−probe signals consist of the same three time components mentioned above with similar relative amplitudes to those observed in Figure 3 (see Table 2). As the acid concentration increases, the intermediate and long component amplitudes decrease. We will use our extended ESPT model to fit the pump−probe signals at 430 and 540 nm. The intermediate time-component in the signal is attributed to the dissociation of the ROH* to form the contact ion-pair that subsequently further evolves to form a separated ion-pair. From the model calculations the transient concentration of the ion-pair is small with a relative amplitude of about 0.25. At low acid concentrations, the intermediate ion-pair transient concentration first increases with an approximately 4 ps time constant and subsequently decays at about 100 ps. At high acid concentrations the ion-pair population is almost constant over time. At very high acid concentrations ($c \geq 1$ M), the ion-pair concentration is time independent for times longer than 5 ps but its amplitude decreases as the acid concentration increases.

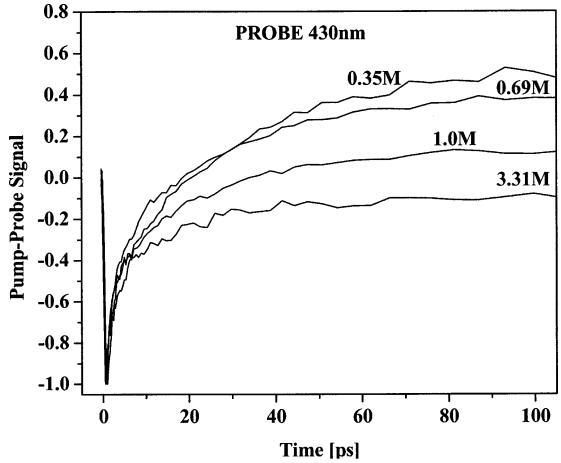

Figure 4. Pump−probe signal of HPTS probed at 430 nm in aqueous solutions containing high concentrations of acids.

TABLE 2: ABC Model Fitting Parameters for a Pump−Probe at 430 nm

$c(HClO_4)$ [M]	$k'_{PT} \times 10^9$ $[s^{-1}]^a$	$k'_r \times 10^9$ $[s^{-1}]^a$	$k_{PT} \times 10^9$ $[s^{-1}]^a$	$k_r \times 10^9$ $[s^{-1}]^a$	$\gamma_1 \times 10^{10}$ $[s^{-1}]^b$	$\gamma_2 \times 10^{11}$ $[s^{-1}]^b$
0.30	35	90	35	10		
1.00	35	105	35	25	2.75	1.68
1.50	35	130	35	50	4.66	2.03
3.00	35	170	35	90	7.81	2.52

[a] Fitting parameter. [b] Calculated by eq a2α (Appendix A).

Time-Resolved Emission. Figure 5a shows the time-resolved emission of the ROH of HPTS measured at 435 nm by the TCSPC technique. Figure 5a shows several TCSPC plots of solutions with large concentrations of $HClO_4$ acid in the range of 0−1.0 M. At low acid concentrations, the amplitude of the long tail is small and arises from the geminate recombination process only. Each of the plots shows biphasic decay with a fast decaying component which has a time constant of about 100 ps at low acid concentrations and shorter time constants at high acid concentrations. For longer times, the ROH emission exhibits a slow exponentially decaying tail with a time constant that is about the excited-state lifetime of both the ROH* and RO^{-}* $\tau \cong 5$ ns. As seen in the figure, the larger the acid concentration, the larger the amplitude of the long time tail.

Figure 5b shows plots of the time-resolved emission of the RO^{-}*, the conjugated base of HPTS measured at 520 nm in the presence of $HClO_4$ in the concentration range 0.174−1.0 M. As seen in the plots, the rise-time of the signal is relatively long for low-acid concentrations while, for high acid concentrations, the signal rise-time is faster and depends on the acid concentration. For comparison we also show the signal of HPTS at low acid concentrations (pH 5) and a basic solution (pH 9), where the excitation is exclusively of the RO^- species, (pK_a(HPTS) = 7.7). For basic pH, the rise-time of the fluorescence signal (∼30 ps) arises from the limited time resolution of the TCSPC technique.

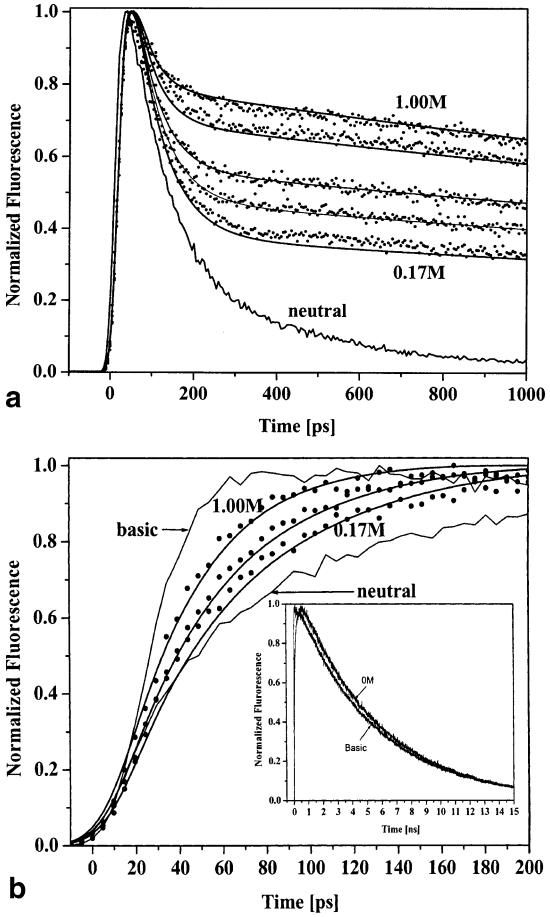

Figure 5. TCSPC time-resolved emission of HPTS solutions with concentrations of $HClO_4$ acid in the range of 0−1.0 M along with computer fits according to the ABC model. (a) Fluorescence was measured near the peak of the ROH band at 435 nm. Acid concentrations, top to bottom: 1 M; 0.8 M; 0.4 M; 0.29 M; 0.17 M; neutral. (b) Fluorescence was measured near the RO^- peak at 520 nm. Acid concentrations: 1 M; 0.4 M; 0.17 M; neutral and basic. Inset: fluorescence of RO^- peak measured at 520 nm of neutral and basic solutions.

Discussion

Analysis of the Acid Effect on Time-Resolved Pump—Probe Experiments. We used the ABC kinetic model (eqs a1 and a2 of appendix A) and the complex expression for the pump−probe signal (eq 3, parts a and b) to fit the experimental pump−probe signals of HPTS probed at 540 and 430 nm in aqueous solutions in the presence of a large concentration of strong acids.

Equation a1, parts $\alpha - \gamma$, of Appendix A provides the time-dependent concentrations of ROH, $RO^-{*}\cdots H_3O^+$, and RO^- according to Scheme 2 of the extended model. The ABC kinetic model assumes that all the rate constants are of the first order. The probability for a proton to recombine with the deprotonated form RO^- and regenerate the reactant excited-state ROH* increases for high acid concentrations. Also, the probability to find an ion-pair $RO^-{*}\cdots H_3O^+$ increases, and hence the recombination rate of ion pairs to form ROH also increases. Thus, the excess proton concentration modifies the recombination rate constants k_r and k'_r of the ABC model that is used in the fit of the pump−probe signal. There are four rate constants in the ABC kinetic model used to describe the short-time window of the pump−probe signal. The first step of the ROH dissociation is described by the forward and back recombination rate constants k'_{PT} and k'_r respectively. We assume that the proton-transfer rate constant, to form the ion-pair k'_{PT}, is independent of the acid presence, while the pseudo-first-order proton recombination rate constant, k'_r, depends on the acid concentration. In the pump−probe experiments, we found that, as the acid concentration increases, the amplitude of both the long-time and intermediate time components decreases. The time dependence concentrations of A, B and C depend on the rate constants. As the acid concentration increases, it modifies the recombination rate constants k_r and k'_r. We used concentration-dependent rate constants $k_r(c_{H^+})$ and $k'_r(c_{H^+})$. Although the rate constants of the ABC model are of the first order, we modify them to be pseudo first order depending linearly on the acid concentration. We used the following expressions for the recombination rate constants:

$$k_r(c_{H^+}) = k_r^{\,0} + k_{rc}(c_{H^+})[H^+] \tag{2a}$$

$$k_r'(c_{H^+}) = k_r' + k_r(c_{H^+}) \tag{2b}$$

The line of reasoning for these expressions is given in Appendices A and B.

For the recombination step of a homogeneous proton with a free excited conjugated base $RO^-{*}$ to form a contact ion-pair

$$H^+ + RO^-{*} \underset{k_{PT}}{\overset{k_r}{\rightleftharpoons}} RO^-{*}\cdots H^+$$

we used $k_r = k^0{}_r + k_{rc}(c_{H^+})$, and confirmed Weller's[3] value $k_{rc}(c_{H^+}) = 5 \times 10^{10}\ M^{-1}\ s^{-1}$ for the second-order rate constant for excited-state recombination of $RO^-{*}$ with homogeneous protons at low acid concentrations. $k_{rc}(c_{H^+})$ depends on the proton diffusion constant and the screening of the Coulomb potential between reactive protons and RO^- by other ions in the solution. Thus, $k_{rc}(c_{H^+})$ decreases as the acid concentration increases (see Appendix B), and $k^0{}_r \approx 2 \times 10^9\ s^{-1}$ is determined from the probability of a geminate proton to recombine to form ROH* in neutral pH solutions. The rate was also computed in our previous paper[23] ($k_{eff} \approx (2 \pm 1) \times 10^9\ s^{-1}$).

Short-Time. Figure 6a shows the plot of the ABC model calculation in a neutral pH solution of $[A]_t$, the protonated form ($[B]_t + [C]_t$), the combined contribution of $RO^-{*}\cdots H_3O^+$ and $RO^-{*}$ as well as the separate contributions of $[B]_t$ ($RO^-{*}\cdots H_3O^+$) and $[C]_t$ ($RO^-{*}$) as a function of time. The rate constants chosen for the plots of Figure 6a are those that best fit the pump−probe signal as well as the TCSPC signals of both ROH and RO^- fluorescence. In Figure 6a, we clearly see the nature of the two reactive step model. The ROH band decays in two phases—a short one of about 4 ps with an amplitude of about 0.3 and a long time component of about 100 ps with amplitude of 0.7. The combined population of the $RO^-{*}\cdots H_3O^+$ and $RO^-{*}$ signals increases in two phases—one of about 4 ps and the other of 100 ps.

Parts b−d of Figure 6 show similar plots of the transient concentration of ROH, $RO^-{*}\cdots H_3O^+$, and $RO^-{*}$ in the presence of 0.5, 1, and 2 M of acid, respectively. As the acid concentration increases, the transient ROH* population, $[ROH^*]_t$, reaches a long tail due to efficient proton recombination. The relative amplitude of the long tail increases with acid concentration. The time-integrated population of the free conjugated base RO^- decreases as the acid concentration increases. The rise-time of RO^- and the decay time of ROH decrease as the acid concentration increases. The decay time of the ion pair population, $[RO^-{*}\cdots H_3O^+]_t$, to form free RO^-, increases as the acid concentration increases. At about $c_{acid} \geq 0.5$ M, the time dependence of the population $[RO^-{*}\cdots H_3O^+]_t$ is quasi-constant

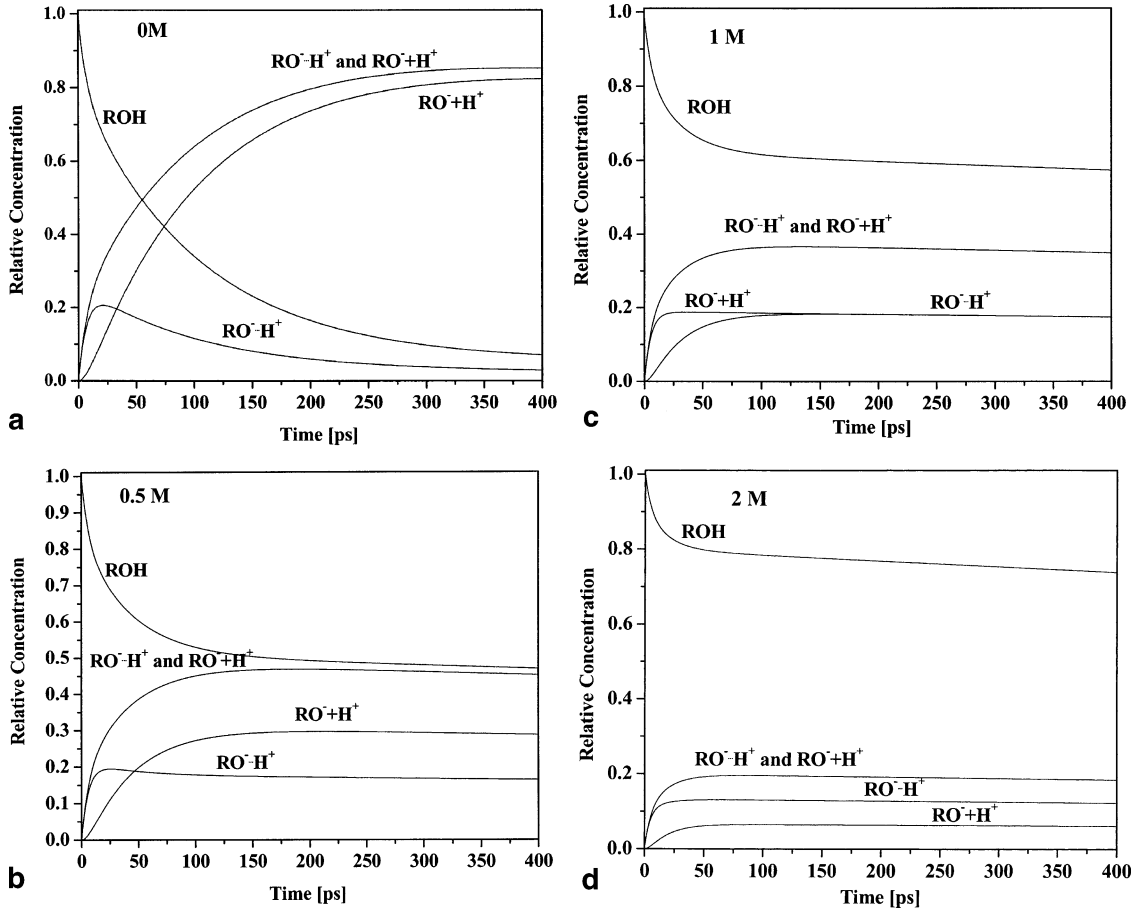

Figure 6. Plot of the ABC model calculation of the protonated form [ROH*], the combined contribution of $RO^{-}{}^{*}\cdots H_3O^{+}$ and $RO^{-}{}^{*}$ as well as the separate contributions of $[RO^{-}{}^{*}\cdots H_3O^{+}]_t$ and $[RO^{-}{}^{*}]_t$ as a function of time, for several acid concentration: (a) 0 M; (b) 0.5 M; (c) 1.0 M; (d) 2.0 M

and decays with the same rate as the excited state $\tau \cong 5$ ns. As the acid concentration further increases, the intermediate contact ion-pair time-integrated concentration decreases. At 2 M, the population fraction decreases from about 0.25 for a neutral solution to about 0.1.

The pump−probe signal of HPTS, measured at 540 nm, in neutral water is approximated by superposition of the ROH absorption, from its first excited state to higher excited states, and the stimulated emission of the ROH form and the RO^{-} form. In the spectral range $\lambda > 500$ nm, the contribution of the emission of the ROH is small and the absorption of $RO^{-}{}^{*}$ to a higher excited state is also small. The pump−probe signal measured at a specific wavelength λ in the long wavelength 520−600 nm range can be approximated by

$$PPS_{\lambda}(t) \propto a_1 \cdot \sigma(\lambda)^{ROH}_{S_1 \rightarrow S_2} c_t^{ROH} - b_1 \cdot \sigma(\lambda)^{RO^-}_{S_1 \rightarrow S_0} [c_t^{RO\cdots H^+} + c_t^{RO---H^+}] + c_1[\exp(-k_{\Delta} t)] \quad (3a)$$

The pump−probe signal measured at 430 nm the signal is given by

$$PPS_{\lambda}(t) \propto a_2 \cdot \sigma(\lambda)^{RO^-}_{S_1 \rightarrow S_2} [c_t^{RO^-\cdots H^+} + c_t^{RO^---H^+}] - b_2 \cdot \sigma(\lambda)^{ROH}_{S_1 \rightarrow S_0} c_t^{ROH} - c_2[\exp(-k_{\Delta} t)] \quad (3b)$$

where *a*, *b*, and c are adjustable amplitudes and $\sigma(\lambda)^{ROH}_{S_1 \rightarrow S_2}$ and $\sigma(\lambda)^{RO-}_{S_1 \rightarrow S_2}$ the absorption cross sections for the excited-state absorption of ROH or RO^{-} to higher excited states. $\sigma(\lambda)^{ROH}_{S_1 \rightarrow S_0}$ and $\sigma(\lambda)^{RO-}_{S_1 \rightarrow S_0}$ are the emission cross sections from $S_1 \rightarrow S_0$ for RO^{-} and ROH. c_t^{ROH}, $c_t^{RO^-\cdots H^+}$, and $c_t^{RO^---H^+}$ are the time-dependent concentrations of the acid form, the contact ion-pair and the solvated ion-pair, respectively. The term $c[\exp(-k_{\Delta} t)]$ probably arises from the solvation dynamics of the reactants and products or vibration energy redistribution and subsequent cooling of the ROH. These processes were also observed in previous studies.[10,11,32]

The main achievement in this paper is shown in Figure 7, parts a and b. Figure 7a shows the experimental pump−probe results of acid solutions of HPTS probed at 540 nm along with the fit of the signal by the extended ESPT model and the time-dependent concentrations calculated by the ABC kinetic model. As seen in Figure 7a, the model fit is rather good for all acid concentrations. Figure 7b shows the pump−probe signal probed at 430 nm along with the model fit. Also, in this case, we are able to fit the signals at all acid concentrations. Table 1 gives the model fitting rate constants of the various pump−probe signals measured at several acid concentrations and probed at 540 nm. The recombination rate constants of eq 3 depend on the acid concentration according to eq 2. The calculated pump−probe signal amplitudes of eq 3a are $a_1 = 1$, $b_1 = 1.65$, and $c_1 = 0.3$. Table 2 contains the model fitting amplitudes for the pump−probe signal, probed at 430 nm. The pump−probe parameters of eq 3b are $a_2 = 1$, $b_2 = 2.6$, and $c_2 = 0.6$.

Long-Time Fluorescence Measurements. Parts a and b of Figure 5 show the plots of the computer fits along with the experimental TCSPC signals of both the ROH measured at 435 nm and the RO^{-} at 520 nm. The computed signals are convoluted with the TCSPC system response of about 35 ps

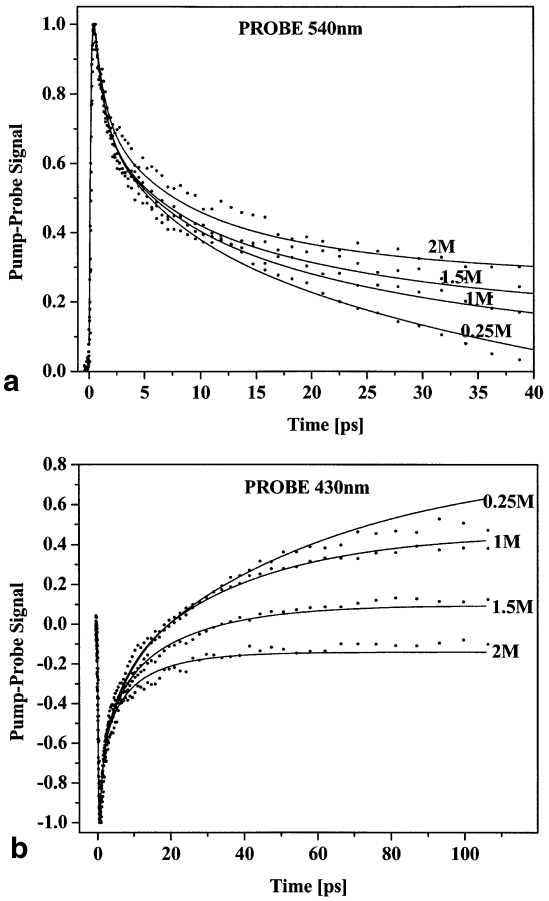

Figure 7. Experimental pump−probe results of acid solutions of HPTS along with the fit of the signal by the ABC model: (a) probing at 540 nm; (b) probing at 430 nm.

since the lifetime of ROH and RO^- are similar, $\tau_f \approx 5.0$ ns. We multiplied the populations in eq 1 of appendix A by $\exp(-t/\tau_f)$. The signal of the ROH fluorescence does not show the short time small amplitude component of about 4 ps observed in the experimental pump−probe signal in Figures 3 and 4 and the computed signal in Figure 7. The rise-time of RO^- of the time-resolved fluorescence signal shows a fast component with amplitude of about 0.2 and a long component of amplitude 0.8 with a rise-time of about 100 ps. The fast component of the RO^-* rise-time cannot be resolved in time due to the 35 ps system response. The overall effect of the slow response of the TCSPC is that the short time component is totally missing in the time-resolved ROH emission measurement while the RO^- signal has an immediate rise-time with an amplitude of about 0.2. As seen in Figure 5a, the short time component of the ROH decay is absent in the experimental TCSPC signal as well as the convoluted computer fit. Figure 5b shows the computer fit to the RO^- signal measured at 520 nm. The rise-time of the RO^- is biphasic with short and long-time components. The fit of the computed signal to the experimental ROH is only good for short times since the ABC cannot accurately reproduce the long time nonexponential fluorescence decay arising from the diffusion assisted geminate recombination step.

Simple AB Dissociation Kinetic Model. To check the necessity to invoke an extended ESPT model that includes the contact ion-pair intermediate, we also compared the experimental results with a simpler model that includes only a single reactive kinetic step (see Scheme 3). The model does not include an intermediate step and an intermediate species like the ion-pair we dealt with in the extended model. The kinetics of the reversible dissociation of HPTS can be described by a simple AB dissociation kinetic model.[33] Consider a photoacid (ROH*), dissociating in a single step (rate coefficient k_d) to produce the excited conjugate base (RO^-*). The latter, in turn, may associate bimolecularly with a proton (rate coefficient k_a) to regenerate the excited acid.

When protons are in great excess, $c \equiv [H^+] \gg [ROH^*]$, and the pseudo-unimolecular recombination rate coefficient is ck_a. In the case of HPTS, the lifetimes of the acid and base are almost equal ($1/k_0 = 1/k'_0$), the reaction is equivalent to AB $\rightleftarrows$ A + B, when we set $[AB] = [ROH^*]\exp(k_0 t)$ and $[A] = [RO^-{}^*]\exp(k_0 t)$. For high acid concentrations ($c > 0.5$ M), we can neglect first-order approximation diffusional effects. From simple chemical kinetics with no diffusional effects, the time dependence of the relative concentration of the acid, given that initially ($t = 0$) only ROH has been excited, is given by

$$\frac{[ROH^*](t)}{[ROH^*](0)} = \frac{e^{-k_0 t}}{1 + cK_{eq}}[e^{-(k_d + ck_a)t} + cK_{eq}] \qquad (4a)$$

$$\frac{[RO^-{}^*](t)}{[RO^-{}^*](0)} = 1 - \frac{[ROH^*](t)}{[ROH^*](0)} \qquad (4b)$$

Here, K_{eq} is the excited-state quasi-equilibrium coefficient given by $K_{eq} = k_a/k_d$. The above solution starts from unity and decays to the equilibrium distribution, $cK_{eq}/(1 + cK_{eq})$, multiplied by the excited-state decay function, $\exp(-k_0 t)$. While the ROH* concentration decays biexponentially, the approach of $[ROH^*]_{(t)}\exp(k_0 t)$ to equilibrium is a single exponential, $\exp[(-1 + cK_{eq})k_d t]$. This solution is at odds with the exact asymptotic solution for reversible diffusion-influenced reactions at long-times, and even with approximate solutions for the short/intermediate-time behavior.[33]

We used eq 4, parts a and b, to fit the "acid" effect on the time-resolved experimental results measured by either the TCSPC time-resolved emission or the pump−probe technique. In general, the fit of the long time measured by TCSPC fluorescence is good while the fit of the short time pump−probe measurements is poor. Figure 8a shows the TCSPC ROH time-resolved emission of HPTS in solutions containing large concentrations of acid, along with the computer fit using eq 4a. In the fitting shown in Figure 8, the forward rate constant $k_d = 10^{10}$ s^{-1} was independent of the acid concentration. The recombination rate constant, k_a, was concentration dependent. It decreases with acid concentration. In a more realistic model, the recombination of a proton with RO^- depends on the diffusion constant and the Coulomb potential between the charged particles. k_a was calculated by eq b4 in Appendix B and accounts for the diffusion and ion-screening effects. The effective recombination reaction rate constant used to fit the experimental data for low acid concentrations, $k_a = 5 \times 10^{10}$ M^{-1} s^{-1}, reduces to about 1.2×10^{10} M^{-1} s^{-1} at a concentration of about 1 M. The relative amplitude of the fluorescence long tail seen in the TCSPC signal of ROH (Figure 8a) depends on the acid concentration and rate constants k_d and k_a. As seen in Figure 8a, the larger the acid concentration the larger the amplitude of the long time tail. Using a concentration- dependent recombination rate constant, k_a, to fit the experimental results gives a rather good fit.

Figure 8b shows the time-resolved emission of HPTS in an aqueous solution containing various amounts of acid measured at 520 nm, near the peak of the RO^-* band, along with the computer fit using the simple AB kinetic model. As seen in the

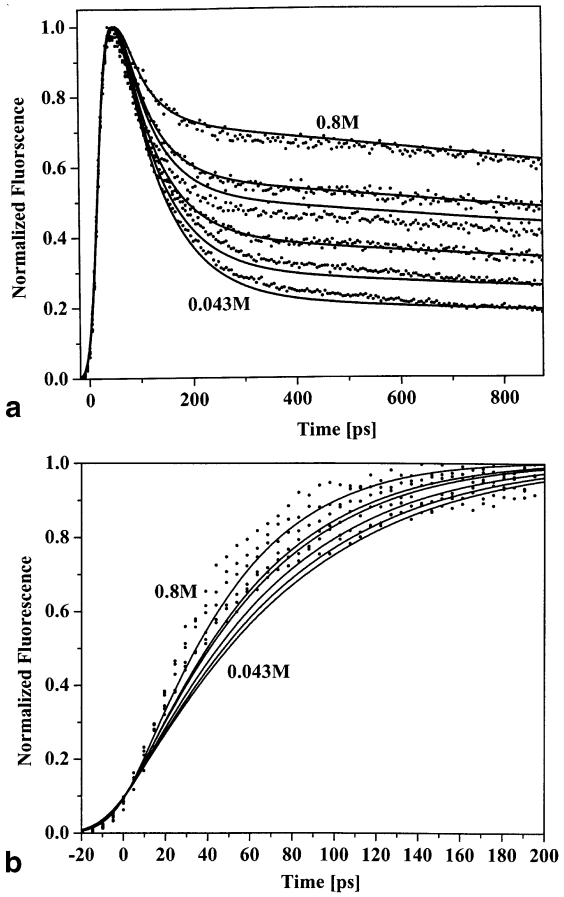

Figure 8. TCSPC time-resolved emission of HPTS in solutions containing large concentrations of acids, along with the simple AB kinetic model computer fit (see text): (a) ROH measured at 435 nm; (b) RO^- measured at 520 nm.

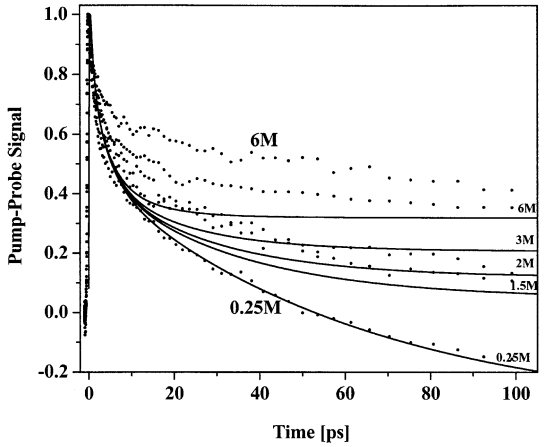

Figure 9. Pump-probe signal of HPTS in a solution containing a strong acid along with a fit using the simple AB kinetic model. Note the large difference between model calculation and experimental results.

figure the fits are rather poor. The rise-time of the model calculation is slower than the experimental results in which the growth time of the emission signal is faster for all acid concentrations. In the calculation, we added a component to the RO^- TCSPC signal, with an amplitude of 0.12, of the ROH signal instrument response to account for the overlap between the ROH and RO^- bands at 520 nm.[30] The reason for the mismatch between the calculated signal and the experimental results lies in the fact that the model does not account for a population of about 0.22 of the intermediate species, the ion-pair, as mentioned above. According to the extended model,

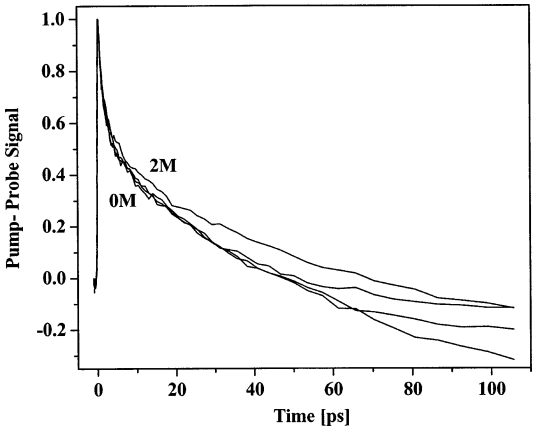

Figure 10. Pump−probe signal (probed at 540 nm) of HPTS in a neutral pH solution (pH ≈ 5) in the presence of various amounts of NaCl salt.

SCHEME 3

$$ROH^* \underset{k_a}{\overset{k_d}{\rightleftharpoons}} RO^{-*} + H^+$$
$$\downarrow k_0 \qquad\qquad \downarrow k_0'$$

the ion-pair is generated within an ultrafast period of about 4 ps and subsequently converts to free RO^-.

The simple kinetic model shown in Scheme 3 can also be used to calculate the short-time window measured by the pump-probe signal of HPTS solutions that contain large acid concentrations. The pump−probe signal measured at 540 or 430 nm consists of three time components, short (<1ps), long (∼100 ps), and intermediate (about 4 ps).

As seen in Figures 3 and 4, when the acid concentration exceeds $c > 0.25$ M, the pump−probe signals, which cover only the first 100 ps, depend on the acid concentration. The pump−probe signals amplitudes of both the long and intermediate time components decrease with increasing acid concentration. At about 3 M of $HClO_4$, the long component seems to almost disappear and the intermediate component amplitude decreases by more than a factor of 2. As seen in parts a and b of Figure 8, we were able to fit the experimental pump−probe signals by the extended ESPT model where the transient concentrations are calculated by the ABC kinetic model, taking into account the pseudo-first-order nature of the recombination rate constants. For high acid concentrations, the value of the recombination rate constants increases, and hence the ROH* concentration increases and the free RO^- concentration decreases. For high acid concentrations, the intermediate species, the contact ion- pair concentration, also decreases with the increase in acid concentration. The simple kinetic model, shown in Scheme 3, does not include an intermediate contact ion-pair. Thus, changes in the RO^- concentration directly affect the photoacid ROH concentration.

To fit the short-time pump−probe signal of a neutral pH HPTS solution with the simple AB kinetic model, we added to eq 3 an additional time component of about $\tau = 4$ ps to account for the intermediate time component with an amplitude of about 0.3 observed in HPTS in a neutral pH solution. The intermediate time component of ∼4 ps seen in Figure 3 can be explained by relating it to a relatively long time solvation process. This relatively long time component contradicts the common knowledge that the longest solvation component of water is about 1 ps. It was observed in several solvation studies of dye molecules in water.

Figure 9 shows an attempt to fit, using the simple AB kinetic model, the pump−probe HPTS signal in acid solutions. The

signal of a 0.25 M acid solution was successfully fit using of eq 4, parts a and b, to calculate the photoacid ROH* and the conjugate base RO^-* time-dependent concentrations and the expression given by eq 3 for the complex contributions of the pump−probe signal. The short time and intermediate time components are added to all the calculations with the same amplitudes and time constants of the fit of the 0.25 M acid solution.

Using eq 4, parts a and b, to calculate the ROH* and RO^-* concentrations as a function of $HClO_4$ concentration fails to fit the pump−probe signals, as clearly seen in Figure 9. The model takes into account the decrease of the long-time amplitude of the pump−probe signal arising from the proton dissociation that takes about 100 ps. The long time component amplitude reduction with the increase of the acid concentration seen in the AB model calculation arises from the proton recombination process for which the terms ck_a (see eq 4a) and cK_{eq} increase linearly with acid concentration. It cannot explain the experimental results seen in Figure 9 showing that as the acid concentration increases the amplitude of the intermediate component decreases. We conclude that the simple AB kinetic model cannot account for the decrease in the amplitude of the intermediate time component of 4 ps with the increase in the acid concentration. The kinetic ABC and extended ESPT models-based transient concentration calculation accounts for the acid effect at both short and long times.

A plausible explanation of part of the strong acid is high concentration effect on the HPTS experimental results may arise from a total different origin—the kinetic salt effect known to influence the kinetics between ions. As a control and complementary experiment, we measured the signals of HPTS in the presence of large concentrations of a univalent salt. In the next subsection, we discuss the results of the "salt" effect on the pump−probe HPTS signal as well as the TCSPC time-resolved emission. We added a large concentration of inert salt to the HPTS solution. As will be seen in the next subsection, the pump−probe signal preserves its shape at all salt concentrations in the range of $0.1 \leq c \leq 2$ M.

The "Salt" Effect. The "acid" effect is accompanied by an additional "salt" effect that complicates the analysis of the experimental data. Strong acids in aqueous solutions dissociate to form ions. A large ion concentration modifies the Coulomb potential between the RO^- and excess protons. We used the Debye−Hückel screened Coulomb potential[34]

$$V(r) = \frac{-R_D \exp[-\kappa_{DH}(r-a)]}{r(1+\kappa_{DH}a)} \qquad (5)$$

with an adjustable Debye−Hückel parameter, κ_{DH}. $1/\kappa_{DH}$ is the radius of the "ionic atmosphere". For a univalent electrolyte, $\kappa_{DH} = Bc^{1/2}$ where for water, $B = 0.33\ M^{-1/2}$. Ionic interaction also leads to a decrease in the diffusion coefficient of ions with increasing ionic strength.[34] We previously detected this effect experimentally for proton geminate recombination with the RO^- of HPTS in a neutral pH solution when an inert salt was introduced.[26]

Figure 10 shows the pump−probe signal probed at 540 nm of HPTS in a neutral pH solution (pH ≈ 5) in the presence of various amounts of NaCl salt. As seen in the figure, even large concentrations of salt (2 M) have only a small effect on the pump−probe signal. This observation is in contrast to the large effect observed on the pump−probe signal in the presence of a high concentration of $HClO_4$. Thus, we exclude the possible interpretation that the "acid" effect on the pump−probe data

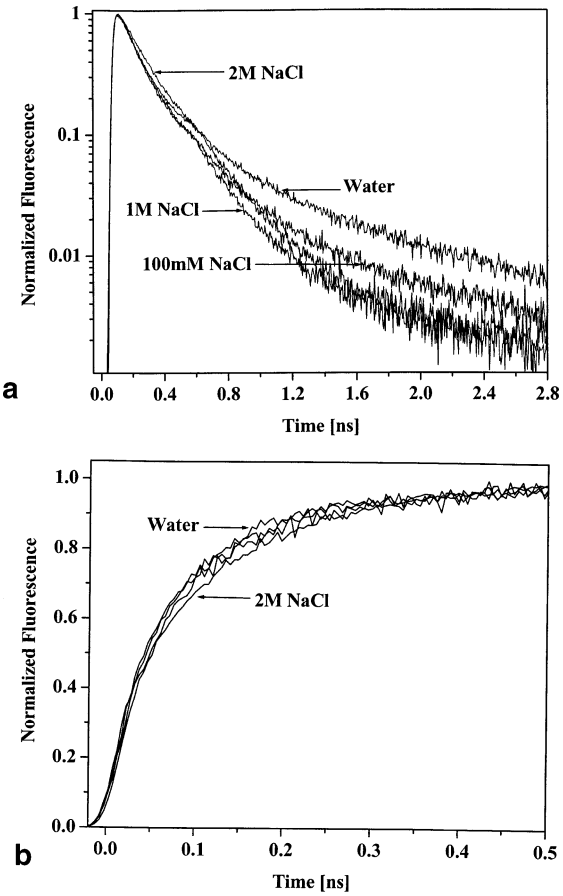

Figure 11. TCSPC time-resolved fluorescence of HPTS: (a) ROH form measured at 435 nm; (b) RO^- emission measured at 520 nm in a solution containing a large amount of NaCl.

arises from the "salt" effect. The results shown in Figures 3 and 4 clearly indicate that the "acid effect" is a genuine effect of an excess proton on the transient concentration of the intermediate species and the concentrations of both ROH and free RO^-.

Parts a and b of Figure 11 show the TCSPC time-resolved fluorescence of ROH and RO^- emission measured at 435 and 520 nm respectively in a neutral pH solution containing a large amount of NaCl. As seen in Figure 11a, in the presence of NaCl, the time-resolved ROH emission decays almost exponentially and the long tail is missing. This is explained by the large electrostatic screening of the Coulomb attraction due to the presence of the salt in the solution. The Debye radius of HPTS RO^- in water is 28 Å. The Coulomb screening by ions reduces the attractive effective potential to such short distances that basically the effective electric attractive potential between the RO^- and the proton reduces to zero. An important conclusion from the almost identical initial slopes of the fluorescence curves of the ROH signal seen in Figure 11a is that the overall proton transfer rate constant is only slightly reduced as the salt concentration increases. This fact confirms the small effect of the NaCl concentration on pump−probe signals as shown in Figure 10.

To summarize the "salt" effect results, the experimental measurements of the "salt" effect show that even large concentrations of NaCl (up to 2 M) only slightly modify the pump−probe signal and hence the proton-transfer rate constants involved in the dissociation process of HPTS are almost independent of the salt concentration. In contrast, the long-time, $t > 100$ ps, geminate recombination rate between the proton and RO^- is strongly affected by the Coulomb screening. At

long times and large salt concentrations ($c > 1$ M), the proton recombination probability decreases dramatically. The main result that concerns the extended model is that salt does not affect the intermediate time component of the pump−probe signal, in contrast to the acid effect, in which large concentrations of acid reduce the intermediate component amplitude to zero.

Steady-State Measurements. To calculate the relative steady-state time integrated emission intensities of ROH and RO^- as a function of the $HClO_4$ concentration shown in Figure 2, we integrate the time dependent concentration of the ROH, $RO^-\cdots H_3O^+$ and RO^- given in eq a1α−a1γ in Appendix A. We used the ABC model to calculate the relative concentrations of the ROH, the intermediate species $RO^-{}^*\cdots H_3O^+$, and the free conjugate base $RO^-{}^*$. At small acid concentrations ($c < 0.1$ M), the steady-state emission of RO^- arises from a large contribution of the long-lived free RO^- and a small contribution of the short-lived intermediate the ion-pair. As the acid concentration increases, the population shifts from the free RO^- toward the photoacid ROH. Also the effective lifetime of the intermediate $RO^-\cdots H_3O^+$ time-dependent concentration increases as the acid concentration increases. As the acid concentration increases, the value of the two recombination rate constants of the ABC model, k'_r and k_r, increase. The details of the time dependence concentrations and the dependence of the recombination rate constants on the acid concentration are given in Appendix A. Figure 2 shows the experimental relative emission intensities of ROH and RO^- (symbols) as a function of the acid concentration along with the calculation using the ABC model of the time integrated combined RO^- emission intensity and that of the ROH.

We also plotted the relative emission intensities of the contact ion-pair $RO^-\cdots H^+$ and the free RO^-. As seen in the figure, the fit of the experimental signal by the ABC model is rather good. For pH < 4, the relative ROH emission is about 0.035 and the $RO^- \sim 0.97$. If we exclude the recombination probability, the relative fluorescence of the ROH is only $\Phi = k_{PT}\cdot\tau \approx 0.019$. The relatively large value of the ROH emission $\Phi = 0.035$ in solution of 6 > pH > 4 arises from the large geminate recombination probability of the positive proton, H_3O^+, with negatively quadruple charged RO^-. As the acid concentration increases, the ROH population increases whereas the RO^- decreases. The rate of population change increases at acid concentrations of about 0.1 M. At 0.1 M, the pseudo-first-order recombination rate constant $k_r = k_{rc}[H_3O^+]$, where $k_{rc} = 5 \times 10^{10}$ M^{-1} s^{-1} and thus $k_r = 5 \times 10^9$ s^{-1}. This large value competes with the dissociation rate constant $k_{PT} = 10^{10}$ s^{-1} to repopulate ROH and hence decrease the RO^- emission intensity. The ion-pair time integrated concentration increases only at high acid concentrations and reaches a maximum value of about 0.2 at about 1 M acid. As the acid concentration further increases, both the ion-pair concentration and the free RO^- decrease, and the emission signal mainly arises from the ROH band.

Conclusions

On the basis of pump−probe measurements of both the ROH and RO^- signals, we developed an extended model for intermolecular excited-state proton transfer (ESPT) to the solvent.[30] The model includes two reactive steps followed by a diffusion-assisted step. The model accounts for the biphasic decay of the pump−probe signals at 520−580 nm (the RO^- emission band) and at the ROH emission band at about 430 nm. In this study, we tested the model by measuring the "acid" effect. We measured the HPTS emission and absorption by steady-state and time-dependent techniques in the presence of large concentrations of strong acids. We found that large concentrations of acids, $c > 0.25$ M, reduces the amplitude of the intermediate short time component of about 4 ps observed in the pump−probe signals. We successfully fit the experimental results with the extended model that includes the acid concentration. The acid concentration modifies, in a consistent manner, the recombination rate constants of the excess proton with RO^- to form the reaction intermediate, the contact ion-pair, and the photoacid (ROH*).

Acknowledgment. This work was supported by grants from the Binational US−Israel Science Foundation, and the James−Franck German−Israel Program in Laser−Matter Interaction.

Appendix A

We used a simple kinetic model[31] to display the main features of the extended model for the ESPT process:

$$A(ROH) \underset{k'_r}{\overset{k'_{PT}}{\rightleftharpoons}} B(RO^-{}^*\cdots H_3O^+) \underset{k_r}{\overset{k_{PT}}{\rightleftharpoons}} C(RO^-{}^* + H_3O^+)$$

where A denotes the excited photoacid ROH*, B the ion-pair $RO^-\cdots H_3O^+$, and C the free diffusing RO^- form and the separated ion-pair.

We successfully used the kinetic ABC model to fit the experimental data of HPTS in a neutral pH aqueous solution.[30] In this study, we found that the model can successfully be used to explain the effect of an acid on the complex dynamics of the dissociation of HPTS. The time-dependent concentrations of A, B, and C are qiven by eqs a1α−γ, respectively.

$$[A]_t = [A]_0\left[\frac{k'_r k_r}{\gamma_1\gamma_2} + \left(\frac{{\gamma_1}^2 - \gamma_1(k'_r + k_{PT} + k_r) + k'_r k_r}{\gamma_1(\gamma_1 - \gamma_2)}\right)e^{-\gamma_1 t} + \left(\frac{{\gamma_2}^2 - \gamma_2(k'_r + k_{PT} + k_r) + k'_r k_r}{\gamma_2(\gamma_2 - \gamma_1)}\right)e^{-\gamma_2 t}\right] \quad (a1\alpha)$$

$$[B]_t = k'_{PT}[A]_0\left[\frac{k_r}{\gamma_1\gamma_2} + \left(\frac{k_{PT} - \gamma_1}{\gamma_1(\gamma_1 - \gamma_2)}\right)e^{-\gamma_1 t} + \left(\frac{k_r - \gamma_2}{\gamma_2(\gamma_2 - \gamma_1)}\right)\right]e^{-\gamma_2 t} \quad (a1\beta)$$

$$[C]_t = k'_{PT}k_{PT}[A]_0\left[\frac{1}{\gamma_1\gamma_2} + \left(\frac{1}{\gamma_1(\gamma_1 - \gamma_2)}\right)e^{-\gamma_1 t} + \left(\frac{1}{\gamma_2(\gamma_2 - \gamma_1)}\right)e^{-\gamma_2 t}\right] \quad (a1\gamma)$$

where

$$\gamma_1 = -\frac{(-(k'_{PT} + k_{PT} + k'_r + k_r) + \Delta}{2} \quad (a2\alpha)$$

$$\gamma_2 = -\frac{(-(k'_{PT} + k_{PT} + k'_r + k_r) - \Delta}{2} \quad (a2\beta)$$

and $\Delta = \sqrt{(k'_{PT}+k_{PT}+k'_r+k_r)^2 - 4(k'_{PT}k_{PT}+k'_r k_r+k'_{PT}k_r)}$.

In the pump−probe experiments, we found that, as the acid concentration increases, the amplitude of both the long-time and intermediate time components decreases. The time dependence concentrations of A, B, and C depend on the rate constants. As the acid concentration increases, it modifies the recombination rate constants k_r and k'_r. We used concentration-dependent rate

constants $k_r(c_{H^+})$ and $k'_r(c_{H^+})$. Although the rate constants of the ABC model are of the first order, we modify them to be pseudo first order depending linearly on the acid concentration. We used the following expressions for the recombination rate constants:

$$k_r(c_{H^+}) = k_r^{\,0} + k_{rc}(c_{H^+})[H^+] \qquad (a3\alpha)$$

$$k_r'(c_{H^+}) = k_r' + k_r(c_{H^+}) \qquad (a3\beta)$$

The line of reasoning for these expressions is given in Appendix B. The diffusion-controlled rate constant for a proton to recombine with an anion with $z = -4$ and a Debye radius of 28 Å is about 2×10^{11} M^{-1} s^{-1}. The intrinsic recombination rate constant, k_r, is smaller and was found to be 5×10^{10} M^{-1} s^{-1}. $k_r(c_H)$ is a diffusion-assisted binary reaction rate constant. The proton diffusion and the attractive potential are concentration dependent and thus also modify the overall recombination rate constant k_r as a function of acid concentration in this simple model. $k_r(c_H)$ is calculated using a diffusion influenced bimolecular reaction based theory. The highlights of such an approximated expression derivation of $k_r(c_{H^+})$ are given in Appendix B.

Appendix B

As a first-order approximation of the dependence of k_r on the acid concentration, we used the long-time asymptotic expression for the rate-constant derived for the bimolecular irreversible diffusion-influenced reaction. Bimolecular irreversible diffusion influenced reactions between donors and acceptors, in the pseudo-unimolecular limit when one reactant is in excess, are the subject of the celebrated "Smoluchowski theory".[27] In the limit that the donor is static, this theory is exact. For zero potential, $U(r) = 0$, it is possible to solve the Debye−Smoluchowski equation and analytically derive an expression for $k(t)$.[35] This is no longer true when $U(r) \neq 0$. In this case, Szabo found an approximate expression for the time-dependent rate constant[36]

$$k(t) = \frac{4\pi D a_e k_r e^{-\beta U(a)}}{k_r e^{-\beta U(a)} + 4\pi D a_e}\left\{1 + \frac{k_{PT} e^{-\beta U(a)}}{4\pi D a_e} e^{\gamma^2 D t}\,\mathrm{erfc}[(\gamma^2 D t)^{1/2}]\right\} \qquad (b1)$$

where $\beta = 1/k_B T$, a is the contact radius ($a \sim 6$ Å), D the diffusion constant and γ is given by

$$\gamma = a_e^{-1}\left(1 + \frac{k_r e^{-\beta U(a)}}{4\pi D a_e}\right) \qquad (b2)$$

erfc is the complementary error function and a_e is an effective radius defined by

$$a_e^{-1} = \int_a^\infty e^{\beta U(r)} r^{-2}\,dr \qquad (b3)$$

Equation b1 is exact when the potential is zero, i.e., $U = 0$ and $a_e = a$. When a potential is introduced, it behaves correctly at both the $t = 0$ and $t = \infty$ limits

$$k(0) = k_r e^{-\beta U(a)},\ k(\infty) = [k(0)^{-1} + k_D^{-1}]^{-1} \qquad (b4)$$

where $k_D = 4\pi D a_e$ is the diffusion-control rate constant. A large ion concentration modifies the Coulomb potential between the RO^- and the excess protons. We used the Debye−Hückel screened Coulomb potential[34]

$$V(r) = \frac{-R_D \exp[-\kappa_{DH}(r - a)]}{r(1 + \kappa_{DH} a)} \qquad (b5)$$

where κ_{DH} is the Debye−Hückel parameter. $1/\kappa_{DH}$ is the radius of the "ionic atmosphere". For a univalent electrolyte, $\kappa_{DH} = BC^{1/2}$ where for water, $B = 0.33$ $M^{-1/2}$. Ionic interaction also leads to a decrease in the diffusion coefficient of ions with increasing ionic strength.[34] We previously detected this effect experimentally for proton geminate recombination with RO^- of HPTS in a neutral pH solution when an inert salt was introduced.[26] We used the long-time $k(\infty)$ expression, given by eq b4 in the calculation of k'_r in the ABC kinetic model.

References and Notes

(1) Bell, R. P. *The Proton in Chemistry*, 2nd ed.; Chapman and Hall: London, 1973.

(2) *Proton-Transfer Reaction*; Caldin E. F., Gold, V., Eds.; Chapman and Hall: London, 1975.

(3) (a) Weller, A. *Prog. React. Kinet.* **1961**, *1*, 189. (b) *Z. Phys. Chem. Neue Folge* **1958**, *17*, 224.

(4) (a) Eigen, M. *Angew. Chem., Int. Ed.* **1964**, *3*, 1. (b) Eigen, M.; Kruse, W.; Maass, G.; De Maeyer, L. *Prog. React. Kinet.* **1964**, *2*, 285.

(5) Ireland, J. E.; Wyatt, P. A. *Adv. Phys. Org. Chem.* **1976**, *12*, 131.

(6) (a) Gutman, M.; Nachliel, E. *Biochim. Biophys. Acta* **1990**, *391*, 1015. (b) Pines, E.; Huppert, D. *J. Phys. Chem.* **1983**, *87*, 4471.

(7) Kosower, E. M.; Huppert, D. *Annu. Rev. Phys. Chem.* **1986**, *37*, 127.

(8) Tolbert, L. M.; Solntsev, K. M. *Acc. Chem. Res.* **2002**, *35*, 1.

(9) Rini, M.; Magnes, B. Z.; Pines, E.; Nibbering, T. J. *Science* **2003**, *301*, 349.

(10) Prayer, C.; Gustavsson, T.; Tarn-Thi, T. H. In *Fast Elementary Processes in Chemical and Biological Systems*; 54th International Meeting of Physical Chemistry; AIP: New York, 1996; p 333.

(11) Tran-Thi, T. H.; Gustavsson, T.; Prayer, C.; Pommeret, S.; Hynes, J. T. *Chem. Phys. Lett.* **2000**, *329*, 421.

(12) Smith, K. K.; Huppert, D.; Gutman, M.; Kaufmann, K. *J. Chem. Phys. Lett.* **1979**, *64*, 22.

(13) Clark, J. H.; Shapiro, S. L.; Campillo, A. J.; Winn, K. J. *J. Am. Chem. Soc.* **1979**, *101*, 746.

(14) Politi, M. J.; Fendler, J. H. *J. Am. Chem. Soc.* **1984**, *106*, 265.

(15) Kolodney, E.; Huppert, D. *Chem. Phys.* **1981**, *63*, 401.

(16) Pines, E.; Huppert, D. *J. Chem. Phys.* **1986**, *84*, 3576.

(17) Pines, E.; Huppert, D.; Agmon, N. *J. Chem. Phys.* **1988**, *88*, 5620.

(18) (a) Ando, K.; Hynes, J. T. In *Structure, Energetics and Reactivity In Aaqueous Solution*; Cramer, C. J., Truhlar, D. G., Eds.; American Chemical Society: Washington, DC, 1994. (b) Ando, K.; Hynes, J. T. *J. Phys. Chem. B* **1997**, *101*, 10464.

(19) Mohammed, O. F.; Dreyer, J.; Magnes, B.-Z.; Pines, E.; Nibbering, E. T. J. *ChemPhysChem* **2005**, *6*, 625.

(20) Pines, E.; Huppert, D. *Chem. Phys. Lett.* **1985**, *116*, 295.

(21) Agmon, N.; Pines, E.; Huppert, D. *J. Chem. Phys.* **1988**, *88*, 5631.

(22) Pines, E.; Huppert, D. *J. Am. Chem. Soc.* **1989**, *111*, 4096.

(23) Pines, E.; Huppert, D.; Agmon, N. *J. Chem. Phys.* **1991**, *85*, 666.

(24) Agmon, N.; Huppert, D.; Masad, A.; Pines, E. *J. Phys. Chem.* **1991**, *96*, 952.

(25) Huppert, D.; Goldberg, S. Y.; Masad, A.; Agmon, N. *Phys. Rev. Lett.* **1992**, *68*, 3932.

(26) Agmon, N.; Goldberg, S. Y.; Huppert, D. *J. Mol. Liq.* **1995**, *64*, 161.

(27) Von Smoluchowski, M. *Ann. Phys.* **1915**, *48*, 1103.

(28) Debye, P. *Trans. Electrochem. Soc.* **1942**, *82*, 265.

(29) Poles, E.; Cohen, B.; Huppert, D. *Isr. J. Chem.* **1999**, *39*, 347.

(30) Leiderman, P.; Genosar, L.; Huppert D. *J. Phys. Chem. A* **2005.** ASAP.

(31) Capellos, C.; Benon, H. K. *Kinetic systems*; Wiley-Interscience: New York, 1972.

(32) Cohen, B.; Leiderman, P.; Huppert, D. *J. Lumin.* **2003**, *102*, 676.

(33) Solntsev, K. M.; Huppert, D.; Agmon, N. *J. Phys. Chem. A* **2001**, *105*, 5868.

(34) Robinson, R. A.; Stokes, R. H. *Electrolyte solutions*, 2nd ed.; Butterworth: London, 1959.

(35) Collins, F. C.; Kimball, G. E. *J. Colloid Sci.* **1949**, *4*, 424.

(36) Szabo, A. *J. Phys. Chem.* **1989**, *93*, 6929.